Liu, J., Li, S., Du, J., Klitis, C., Du, C., Mo, Q., Sorel, M., Yu, S., Cai, X., & Wang, J. (2016). Performance evaluation of analog signal transmission in an integrated optical vortex emitter to 3.6-km few-mode fiber system. *Optics Letters*, *41*(9), 1969-1972. https://doi.org/10.1364/OL.41.001969

Performance evaluation of analog signal transmission in an integrated optical vortex emitter to 3.6 km few-mode fiber system

JUN LIU,[1,+] SHIMAO LI,[2,+] JING DU,[1,+] CHENG DU,[3] QI MO,[1,3] MARC SOREL,[4] SIYUAN YU,[2,5] XINLUN CAI,[2,*] JIAN WANG[1,*]

[1] *Wuhan National Laboratory for Optoelectronics, School of Optical and Electronic Information, Huazhong University of Science and Technology, Wuhan 430074, Hubei, China.*
[2] *State Key Laboratory of Optoelectronic Materials and Technologies and School of Physics and Engineering, Sun Yatsen University, Guangzhou 510275, China.*
[3] *Fiberhome Telecommunication Technologies Co. Ltd, Wuhan 430074, China.*
[4] *School of Engineering, University of Glasgow, Rankine Building, Oakfield Avenue, Glasgow G12 8LT, UK.*
[5] *Department of Electrical and Electronic Engineering, University of Bristol, University Walk, Bristol, BS8 1TR.*
+These authors contributed equally to this work.
**Corresponding author: caixlun5@mail.sysu.edu.cn, jwang@hust.edu.cn*

We experimentally demonstrate and evaluate the performance of analog signal transmission system with photonic integrated optical vortex emitter and 3.6 km few-mode fiber (FMF) link using OAM modes. The device is capable of emitting vector optical vortices carrying well-defined, and quantized OAM modes with topological charge *l*=-2 and 2 carrying analog signal. After propagating through 3.6 km FMF, we measure the spurious free dynamic range (SFDR) of the second-order harmonic distortion (SHD). © 2015 Optical Society of America

OCIS codes: *(050.4865) Optical vortices; (070.1170) Analog optical signal processing, (130.3120) Integrated optics devices.*

A light beam carrying orbital angular momentum (OAM) is characterized by a helical-phase front of$\exp(il\theta)$, in which $l$is the topological charge number, and θ refers to the azimuthal angle. For the helical phase structure, the OAM carrying beam is twisted and features a doughnut intensity profile due to the phase singularity [1]. In 1992, Allen et al. indicated that OAM beam has the discrete value of $l\hbar$ per photon in the propagation direction, where $\hbar$ is the reduced Planck constant [2]. Since then, OAM beam has been employed to explore a variety of novel natural phenomena such as particle trapping, imaging, and quantum information processing, and so on [3-6]. Very recently, the distinct features are unlimited charge values of OAM and intrinsic orthogonality among different OAM states facilitating an alternative multiplexing technique i.e. OAM-division multiplexing (ODM). ODM utilizing the orthogonal OAM mode basis could provide an alternative multiplexing technique in few-mode fibers to further efficient optical communications applications. Lots of research efforts have been devoted to both free-space and fiber-optical communication systems by employing OAM multiplexing to increase transmission capacity and spectral efficiency [7-15].

However, in most of previous works, complex and bulky optical OAM emitter were used which are slow to respond, and cumbersome. This severely limits the prospect of its wide use in future practical systems. In this scenario, a laudable goal would be to develop a micrometer-sized OAM emitter [16]. Meanwhile, the signals carried by OAM modes are digital signal such as m-ary phase-shift keying (m-PSK) and m-ary quadrature amplitude modulation (m-QAM) in most of the OAM transmission experiments [17, 18]. In fact, analog signal transmissions have been developed miscellaneous applications, for instance, broadband wireless access networks, sensor networks, radar systems, remote or phased array antennas, and radio-over-optical transmission systems [18-21]. Recently, analog signal transmission in a free-space OAM multiplexing system by two spatial light modulators (SLMs) was reported [22]. Considering the recent developments of OAM transmission in digital signal transmissions to explore the space dimension of a light beam, it would be also interesting to study the impact of OAM modes on analog signal transmissions of a chip to fiber link.

In this Letter, we experimentally demonstrate and evaluate the performance of analog signal transmission system with photonic integrated optical vortex emitter and 3.6 km few-mode fiber (FMF) link using OAM modes. The device is capable of emitting vector optical vortices carrying well-defined, and quantized OAM. Using this device, we generate two OAM modes with topological charge $l = -2$ and 2carrying analog signal and the two modes propagate in a 3.6km FMF. We measure the spurious free dynamic range (SFDR) of the second-order harmonic distortion (SHD) which is important factor used to estimate the analog link performance.

The experimental setup of analog signal transmission system with photonic integrated optical vortex emitter and 3.6 km FMF link is shown in Fig. 1. At the transmitter side, the output of a tunable laser is injected to an intensity modulator (IM). The light source is modulated by a 3-GHz radio frequency (RF) in the IM, and then amplified by an erbium doped fiber amplifier (EDFA). A polarization controller (PC) is used to launch light in the quasi-TE mode before the signal is coupled into the input waveguide of the micro-ring resonator, and the power is monitored by a power meter placed at the output port of the waveguide. For the state of polarization (SOP) of the source WGMs and the angular grating structure are both cylindrically symmetric, the radiated beams should maintain this symmetry and should be cylindrical vector (CV) beams of which the Jones vector E_{CV} can be

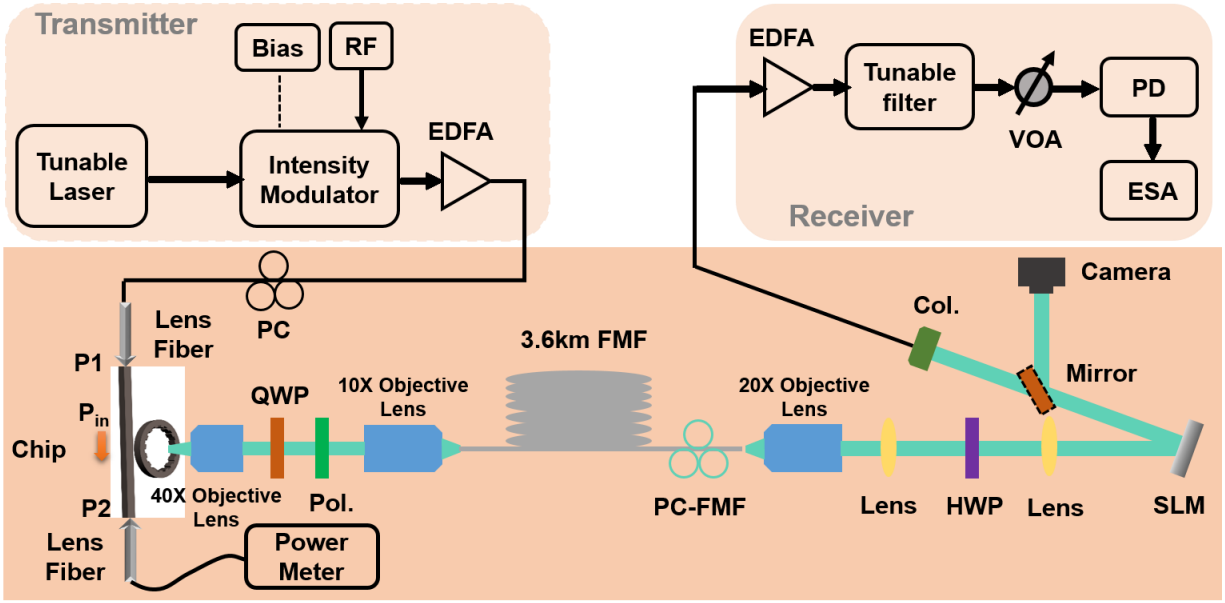

Fig. 1. Experimental setup of analog signal transmission system with photonic integrated optical vortex emitter and 3.6 km FMF link. RF: radio frequency. PC: polarization controller. EDFA: erbium-doped fiber amplifier. QWP: quarter-wave plate. Pol.: polarizer. FMF: few mode fiber. PC-FMF: polarization controller on few mode fiber. HWP: half-wave plate. SLM: spatial light modulator. Col.: collimator. VOA: variable optical attenuator. PD: photodetector. ESA: electric spectrum analyzer.

written as $E_{CV} = \begin{pmatrix} -\sin\theta \\ \cos\theta \end{pmatrix} \exp(il\theta)$. Thus, it can be described as the superposition of two orthogonal scalar vortices, as E_{CV} can be further decomposed into $E_{CV} = \frac{i}{2}\begin{pmatrix} 1 \\ -i \end{pmatrix} \exp i[(l+1)\theta] - \frac{i}{2}\begin{pmatrix} 1 \\ i \end{pmatrix} \exp i[(l-1)\theta]$, which consists of a right-hand circularly polarized (RHCP) beam with topological charge of $l+1$ and a left-hand circularly polarized (LHCP) beam with $l-1$ [16]. After passing through the quarter-wave plate (QWP), the LHCP beam and RHCP beam are converted to two orthogonal linearly polarization beams. Then the linearly polarized OAM beam we need is picked out by a polarizer. In the experiment, we choose OAM_2 at a wavelength of 1531.91 nm and OAM_{-2} at a wavelength of 1556.56 nm. The picked out OAM beams are coupled into the FMF by a 10X objective lens and then propagating through the 3.6 km FMF. The polarization controller (PC) on the FMF (PC-FMF) is adjusted to obtain the OAM states at the FMF input with the smallest possible cross-talk. The OAM beam is collimated by a 20X objective lens after propagating through the fiber and then demodulated by the SLM loaded with a reverse phase pattern. The half-wave plate (HWP) is used to adjust the polarization of the output light of FMF to polarization of the SLM. Finally, the demodulated Gaussian-like beam is coupled into single mode fiber (SMF) for detection. At the receiver side, after being amplified by EDFA and attenuated by VOA, the signal is sent to a photo-detector (PD) and then measured by an electric spectrum analyzer (ESA).

We first measure the intensity profiles of the emitted vector vortex modes. Figure 2 (a) and (c) show the intensity profiles of OAM_2 at a wavelength of 1531.91 nm and OAM_{-2} at a wavelength of 1556.56 nm after decomposition by the QWP and polarizer respectively. The interference patterns of

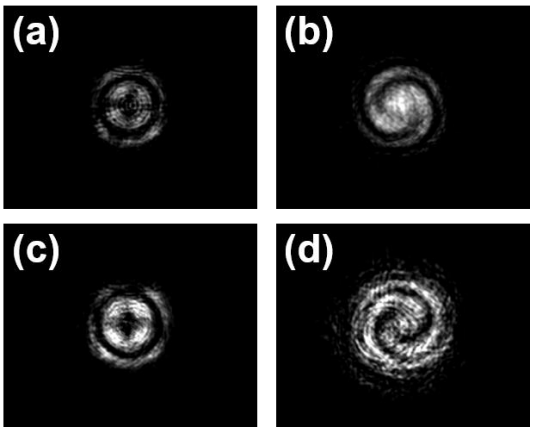

Fig. 2. (a) Measured intensity profile of OAM_2 at a wavelength of 1531.91 nm after decomposition. (b) Measured interference pattern of OAM_2 at a wavelength of 1531.91 nm with a reference Gaussian beam. (c) Measured intensity profile of OAM_{-2} at a wavelength of 1556.56 nm after decomposition. (d) Measured interference pattern of OAM_{-2} at a wavelength of 1556.56 nm with a reference Gaussian beam.

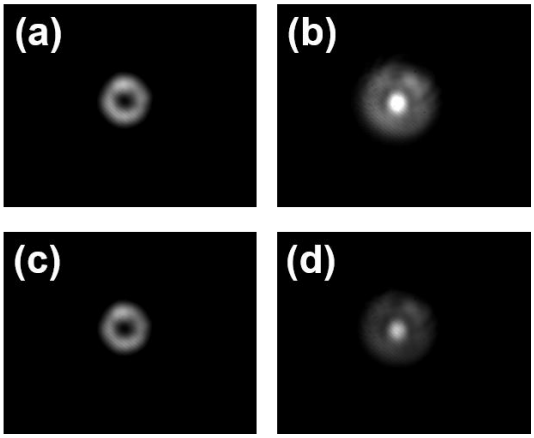

Fig. 3. Measured intensity profiles of (a) OAM_2 at a wavelength of 1531.91 nm after propagating through 3.6 km FMF, (b) demodulation of OAM_2 at a wavelength of 1531.91 nm after SLM, (c) OAM_{-2} at a wavelength of 1556.56 nm after propagating through 3.6 km FMF (d) demodulation of OAM_{-2} at a wavelength of 1556.56 nm after SLM.

these two modes are illustrated in Fig. 2 (b) and (d) correspondingly. The polarization of the reference Gaussian beam is -45° and 45° with respect to the fast axis of QWP.

We also measure the intensity profiles of the two modes after propagating through the 3.6 km FMF. The intensity profiles of OAM_2 at a wavelength of 1531.91 nm and OAM_{-2} at a wavelength of 1556.56 nm after propagating through 3.6 km is demonstrated in Fig. 3 (a) and (c) respectively. Figure 3 (b) and (d) show the intensity profiles of the demodulation of these two modes after modulated by the SLM loaded with a reverse phase pattern.

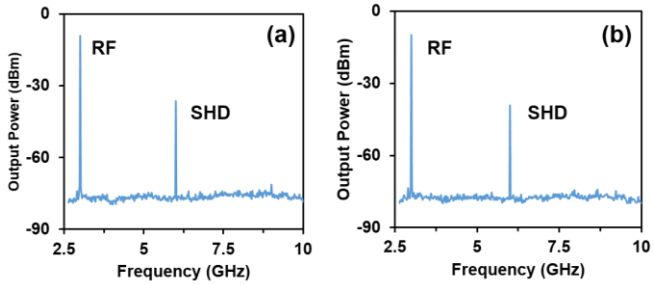

Fig. 4. (a) Measured RF spectra of RF carrier and SHD by ESA at a wavelength of 1531.91 nm before the chip to FMF link. (b) Measured RF spectra of RF carrier and SHD by ESA at a wavelength of 1556.56 nm before the chip to FMF link.

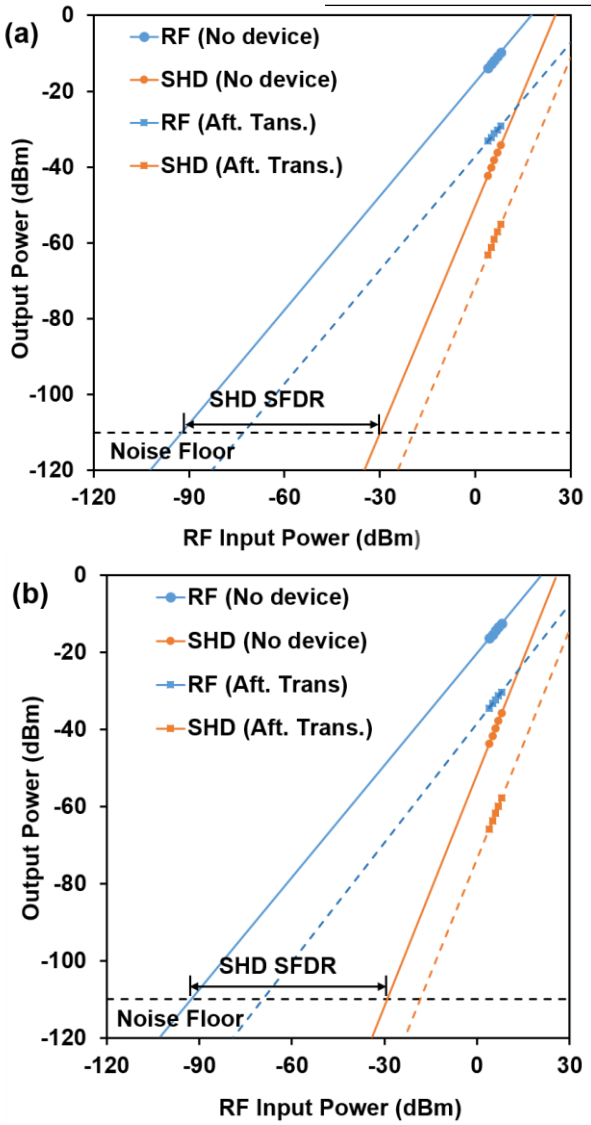

Fig. 5. Measured output power of RF carrier and distortions as a function of the RF input power of (a) OAM_2 at a wavelength of 1531.91 nm and (b) OAM_{-2} at a wavelength of 1556.56 nm, respectively.

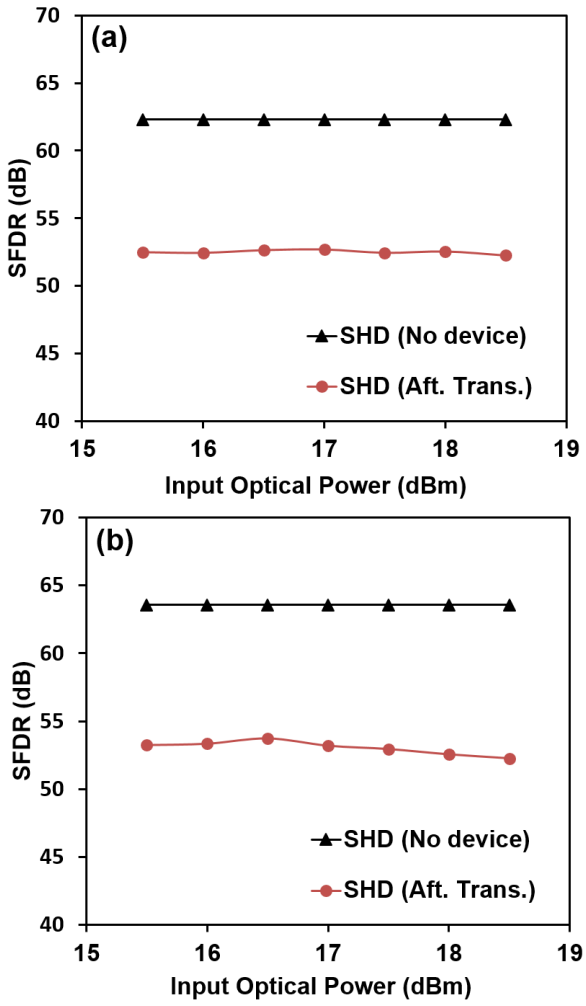

Fig. 6. (a) Measured SHD SFDR versus input signal power of OAM_2 at a wavelength of 1531.91 nm. (b) Measured SHD SFDR versus input signal power of OAM_{-2} at a wavelength of 1556.56 nm.

Then we evaluate the performance of analog signal transmission in optical vortex emitter and 3.6 km FMF link using OAM modes. Figure 4 (a) and (b) indicate measured RF spectra by ESA at a wavelength of 1531.91 nm and 1556.56 nm before the chip to FMF link respectively.

To further analyze the performance of analog signal transmission in optical vortex emitter and 3.6 km FMF link, we measure the output power of the RF carrier and distortions as a function of the RF input power of OAM_2 at a wavelength of 1531.91 nm and OAM_{-2} at a wavelength of 1556.56 nm in Fig. 5 (a) and (b) respectively. The input power of the optical signal is about 15dB. We can see that the analog transmission penalty is induced after transmission over the optical vortex emitter and 3.6 km FMF link. SFDR is an important common judgment criteria to measure the linearity level of an analog link [23, 24]. SFDR is defined by the RF input power range at the left and right boundaries of which the fundamental RF power and SHD/THD power are equal to the noise floor [25, 26]. In generally, a higher SFDR system facilitates a more linear signal transmission. SFDRs can be gained by measuring the intercepting points of output power curves (RF carrier, SHD, THD) and the noise floor. As shown in Fig. 5 (a), for the OAM_2 at a wavelength of 1531.91 nm, the SDH SFDRs before and after the chip to FMF link are 63.57 and 53.25 dB respectively. As depicted in Fig. 5 (b), for the OAM_{-2} at a wavelength of 1556.56 nm, the SDH SFDRs before and after the chip to FMF link are 62.3 and 52.5 dB respectively. A 10 dB degradation of SHD SFDRs are observed for both two modes after transmission in optical vortex emitter and 3.6 km FMF link. The notable reduction of SHD SFDR is induced by two parts. First, the optical transmission loss plays an important role. The transmission loss is up to about 55 dB mainly induced by the emission loss of vortex emitter, coupling loss from free-space to FMF, coupling loss from free-space to single mode fiber (SMF) and optical components such as objective lens, SLM and so on. Second, the SHD SFDR degrades due to the notch filtering effect of the vortex emitter. The sideband caused by RF carrier falls into the 3-dB bandwidth region of the vortex emitter, especially near the notch resonance wavelength. In this case, the vortex emitter actually functions as a filter to eliminate the output fundamental frequency sideband (output RF carrier), while the high-order harmonic sidebands (SHD) survive.

In order to fully investigate the analog signal transmission in the 3-dB bandwidth region near the resonance wavelength, we change the input power from 15.5dBm to 18.5dBm. Figure 6(a) and (b) plot the relationship between SHD SFDR and input power of OAM_2 at a wavelength of 1531.91 nm and OAM_{-2} at a wavelength of 1556.56 nm respectively. One can see that the SHD SFDR varies slightly as the optical input power increasing or even decreases as the input power increasing of OAM_{-2} at a wavelength of 1556.56 nm shown in Fig. 6 (b). Generally, the SHD SFDR should increase with the input optical power. In order to explain these interesting phenomena, we measure the radiation and transmission spectrum of the vortex emitter when the optical input power is 15 dB, 16dB, 17dB, 18 dB respectively as shown in Fig. 7 (a)-(d) by scanning input laser wavelength. The insert red point represents the input wavelength of 1531.91 nm and 1556.56 nm. We can see that the resonance wavelength move towards to longer wavelength as the optical power increasing. This explains that the SHD SFDR stays the same as the input power increasing.

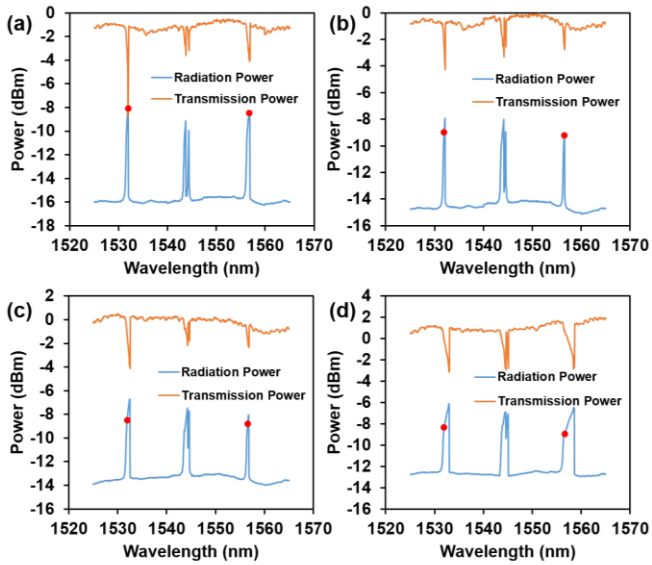

Fig. 7. Measured radiation and transmission spectrum for a device with a radius of 14 μm when the input power is (a) 15 dB, (b) 16dB, (c) 17 dB, and (d) 18 dB respectively.

In conclusion, we experimentally demonstrate and evaluate the performance of analog signal transmission system with photonic integrated optical vortex emitter and 3.6 km few-mode fiber (FMF) link using OAM modes. Two OAM modes are transmitting through the link and we utilize SHD SFDR to evaluate the performance of the analog link. The influences of input signal power on the analog signal transmission are analyzed in detail in the experiment. For relatively high input signal power, it is interesting to note that the analog signal transmission might also be affected by the nonlinearity-induced resonance wavelength shift of the vortex emitter with the increase of input signal power.

Funding. The 973 Program (2014CB340004, 2014CB340003, 2014CB340001); National Natural Science Foundation of China (NSFC) (11274131, 11574001, 61222502); Program for New Century Excellent Talents in University (NCET-11-0182); Wuhan Science and Technology Plan Project (2014070404010201); seed project of Wuhan National Laboratory for Optoelectronics (WNLO).

References

1. A. M. Yao and M. J. Padgett, Adv. Opt. Photon. **3**, 161 (2011).
2. L. Allen, M. W. Beijersbergen, R. Spreeuw, and J. P. Woerdman, Phys. Rev. A **45**, 8185 (1992).

3. D. Grier, Nature **424**, 810 (2003).
4. M. Padgett, R. Bowman, Nat. Photonics **5**, 343 (2011).
5. S. Fürhapter, A. Jesacher, S. Bernet, and M. Ritsch-Marte, Opt. Express **13**, 689 (2005).
6. A. Mair, A. Vaziri, G. Weihs, and A. Zeilinger, Nature **412**, 313 (2001).
7. J. Wang, J.-Y. Yang, I. M. Fazal, N. Ahmed, Y. Yan, H. Huang, Y. Ren, Y. Yue, S. Dolinar, and M. Tur, Nat. Photonics **6**, 488 (2012).
8. A. E. Willner, J. Wang, and H. Huang, Science **337**, 655 (2012).
9. N. Bozinovic, Y. Yue, Y. Ren, M. Tur, P. Kristensen, H. Huang, A. E. Willner, and S. Ramachandran, Science **340**, 1545 (2013).
10. A. Willner, H. Huang, Y. Yan, Y. Ren, N. Ahmed, G. Xie, C. Bao, L. Li, Y. Cao, and Z. Zhao, Adv. Opt. Photon. **7**, 66 (2015).
11. J. Wang, S. Li, C. Li, L. Zhu, C. Gui, D. Xie, Y. Qiu, Q. Yang, and S. Yu, in Optical Fiber Communication Conference (OFC2014), paper W1H. 4. (2014).
12. H. Huang, G. Xie, Y. Yan, N. Ahmed, Y. Ren, Y. Yue, D. Rogawski, M. J. Willner, B. I. Erkmen, and K. M. Birnbaum, Opt. Lett. **39**, 197 (2014).
13. J. Wang, S. Li, M. Luo, J. Liu, L. Zhu, C. Li, D. Xie, Q. Yang, S. Yu, and J. Sun, in European Conference and Exhibition on Optical Communication (ECOC2014), paper Mo.4.5.1 (2014).
14. A. Wang, L. Zhu, J. Liu, C. Du, Q. Mo, and J. Wang, Opt. Express **23**, 29457 (2015).
15. 21. J. Wang, J. Liu, X. Lv, L. Zhu, D. Wang, S. Li, A. Wang, Y. Zhao, Y. Long, J. Du, X. Hu, N. Zhou, S. Chen, L. Fang, and F. Zhang, in European Conference and Exhibition on Optical Communication (ECOC2015), paper Th.2.5.4 (2015).
16. X. Cai, J. Wang, M. J. Strain, B. Johnson-Morris, J. Zhu, M. Sorel, J. L. O'Brien, M. G. Thompson, and S. Yu, Science **338**, 363 (2012).
17. P. J. Winzer, IEEE Leos Newsletter **23**, 4 (2009).
18. J. D. Downie, J. Hurley, J. Cartledge, S. Bickham, and S. Mishra, Opt. Express **19**, B96 (2011).
19. J. P. Yao, J. Lightwave Technol. **27**, 314 (2009).
20. H. Kosek, Y. He, X. Gu, and X. N. Fernando, J. Lightwave Technol. **25**, 1401 (2007).
21. J. Du and J. Wang, Opt. Lett. **40**, 1181 (2015).
22. S. Li and J. Wang, Opt. Lett. **40**, 760 (2015).
23. C. H. Cox, *Analog optical links: theory and practice* (Cambridge University Press, 2006).
24. W. S. Chang, *RF photonic technology in optical fiber links* (Cambridge University Press, 2002).
25. W. B. Bridges and J. H. Schaffner, IEEE Trans. Microwave Theor. Tech. **43**, 2184 (1995).
26. C. H. Cox III, E. Ackerman, G. E. Betts, and J. L. Prince, IEEE Trans. Microwave Theory Tech. **54**, 906 (2006).